ANALYTICAL, NUMERICAL AND EXPERIMENTAL INVESTIGATION OF THE DYNAMIC BEHAVIOR OF A PROTOTYPE FOR A STOCKBRIDGE DAMPER

Thiago de Freitas Pinto, thiagof.pinto@hotmail.com
Anna Carla Araujo, annaaraujo@cefet-rj.br
Av. Maracanã, 485 – E317– Maracanã – Rio de Janeiro – RJ
Departamento de Engenharia Mecânica - CEFET/RJ
Programa de Pós-Graduação de Engenharia Mecânica e Tecnologia de Materiais – PPEMM - CEFET/RJ

Carlos Frederico Trotta Matt, cftmatt@cepel.br
Electric Power Research Center (CEPEL), Department of Equipment and Installations
Avenida Horário 354, Cidade Universitária, Ilha do Fundão, Rio de Janeiro, RJ, Brazil, 21941-911

Abstract. *Stockbridge damper is a dynamic absorber attached to transmission line conductors in order to suppress their amplitudes of vibration induced by the wind. In order to understand the complex dynamic behavior of a typical Stockbridge damper and to further develop an optimized shape and material to increase the effectiveness of the absorber, a series of numerical and experimental simulations must be done. In the current work, a cantilever beam carried at the free end a tip mass slender in the axial direction was manufactured, experimented and simulated. Such cantilever beam prototype resembles a typical Stockbridge damper though the geometrical complexity of the wire cable has not been considered in this preliminary investigation. The governing equations for the dynamic behavior of the prototype, under some set of simplifying assumptions, are set forth and analytically solved. Numerical simulations using the commercial finite-element software ANSYS are also performed with the full three-dimensional prototype model, relaxing some simplifying hypotheses adopted in the analytical treatment. The analytical and numerical results are finally compared with measurements obtained during laboratory tests performed with the prototype.*

Keywords*: Stockbridge damper; FEM simulation; Dynamic absorber; Mechanical modeling*

1. INTRODUCTION

The reliability of a high-voltage transmission line system depends largely on the integrity of its overhead conductors. Overhead conductors are subjected to many different mechanical and electrical phenomena in the field. The damages associated with the mechanical vibrations induced by the wind are one of the main causes for forced interruptions in the supply of electric energy. These wind-induced vibrations are caused by the periodic vortex-shedding phenomenon behind the wake of the conductor and are commonly referred to as aeolian vibrations. The vortex-shedding phenomenon produces a pressure difference between the top and the bottom sides of the conductor which induces an alternating lift force with the same frequency as that of the vortex shedding in the wake. These vibrations arise for wind speeds in the range from 1 m/s to 8 m/s, the frequencies expected lie within the range from 5 Hz to 50Hz and the vibration amplitudes are of the order of the conductors' diameter or less (Wagner *et al.*, 1973). If not properly damped, when the predominant vortex-shedding frequency coincide with one of the resonance or natural frequencies of the conductor, the bending stresses and strains may become too high and may lead to severe fatigue damages at the conductor clamps, leading to the complete rupture of the conductor.

Overhead conductors possess very low internal damping in the frequency range expected for aeolian vibrations in the field. Modifications in the vortex-shedding frequency by introducing perturbations in the wind flow have been proved to be not a good strategy because the conductors possess a large number of resonance frequencies closely spaced. Hence, the best strategy verified has been to attach dynamic absorbers to the conductors in order to remove part of the energy input by the wind, as indicated in Fig. 1. Stockbridge dampers are the most widely used dynamic absorbers attached to transmission line conductors in order to suppress the wind-induced vibrations and, consequently, to minimize the susceptibility of conductors to fatigue damages.

Stockbridge dampers, shown in Fig. 1, generally comprise two inertial masses or counterweights resiliently suspended at the tips of a flexible steel wire cable, commonly referred to as messenger cable, and attached to the conductor at its midpoint through a rigid bolted clamp. In the majority of Stockbridge dampers available at the market, the messenger cable comprises six or eighteen wires helically wrapped around a central straight wire; the wires are normally made of galvanized steel. The purpose of these devices is to absorb part of the energy input by the wind so as to drop down the vibration amplitudes to a security level. Mechanical energy is also dissipated in these devices due to the friction among the wires of the messenger cable during its bending vibrations. When a transmission line conductor equipped with Stockbridge dampers is subjected to forced vibrations (as in the field due to wind), these dampers interact with the conductor by exerting a transverse force and a bending moment at the attachment point. The concentrated transverse force and bending moment may increase too much the local curvature of the conductor leading to large

stresses and strains in the neighborhood of these attachment points (Hagedorn, 1982). Hence, accurate predictions of the dynamic behavior of such damping devices become an important task.

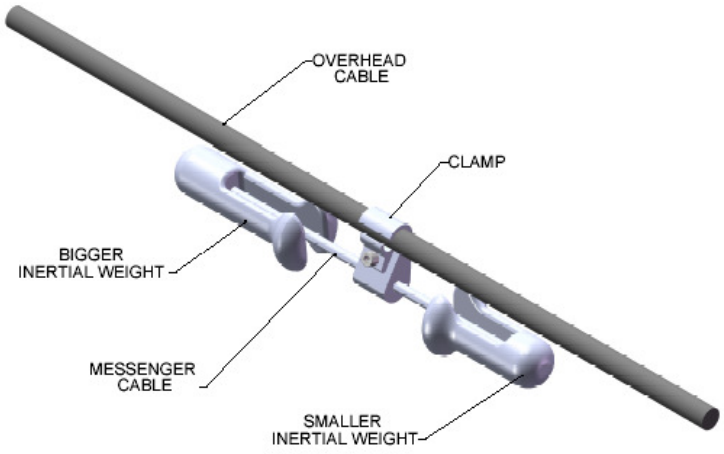

Figure 1. A typical Stockbridge damper attached to an overhead conductor.

Although Stockbridge dampers are easily manufactured, experimental tests performed on a laboratory indicate that these devices possess a quite complex dynamic behavior (Varella *et al.*, 2007). As a first step towards the understanding of the dynamic behavior of a typical Stockbridge damper, in the current work, a simpler prototype resembling a Stockbridge damper is to be analyzed. The prototype comprises a uniform steel cantilever beam with circular cross-section carrying a tip mass slender in the axial direction, schematically illustrated in Fig. 2. The tip mass is made of the same steel as the beam and its gravity center does not coincide with its attachment point to the uniform beam. The major difference between the prototype investigated here and a typical Stockbridge damper relies on the cantilever uniform beam, whose stiffness and damping properties are distinct from the corresponding ones of an actual messenger cable.

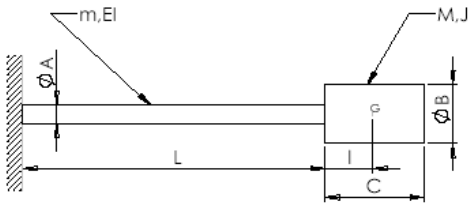

Figure 2. The prototype for a Stockbridge damper investigated in the current work.

The dimensions of the prototype are indicated on Tab. 1.

Table 1. Prototype dimensions (the symbols are indicated on Fig. 2).

Dimension	Value (mm)
ϕ_A	9
ϕ_B	29
C	49
L	149

2. BRIEF LITERATURE REVIEW

Previous researchers have also investigated the dynamic behavior of a cantilever beam carrying a tip mass at the free end. For instance, the exact frequency equation for a uniform cantilever beam carrying a concentrated tip mass without moment of inertia was considered by Pipes (1958), Prescot (1946), Temple and Bickley (1956) and Parnell and Cobble (1976). Durvasula (1965) derived the exact frequency equation for free vibrations of a uniform cantilever beam carrying a tip mass with concentrated moment of inertia. However, the concept of a concentrated mass or moment of inertia is often violated when the tip mass is slender in the axial direction and the attachment point does not coincide

with the gravity center of the tip mass, as is the case for the prototype investigated here and for a typical Stockbridge damper. In these situations, the boundary conditions at the free end of beam must be modified accordingly which increases the complexity of the problem. By using perturbation expansion techniques, Rhama Bhat and Wagner (1976) derived approximate equations to compute the undamped natural frequencies of a cantilever beam carrying a tip mass slender in the axial direction. The numerical results obtained by those authors for the natural frequencies were tabulated for selected values of non-dimensional parameters, which represent ratios between the inertia and stiffness values of the tip mass and of the beam. It is worthwhile to mention that the numerical results obtained by Rhama Bhat and Wagner (1976) lack accuracy when the hypothesis $\varepsilon \equiv l/L << 1$ (see Fig. 2) is not fulfilled.

Two major improvements are proposed in the current work for the theoretical modeling of the prototype shown in Fig. 2. First, an exact frequency equation is derived which allows one to compute the natural frequencies for the cantilever beam-tip mass system; such frequency equation remains accurate even when the hypothesis $\varepsilon \equiv l/L << 1$ is violated. Second, one derives an analytical expression for the transmissibility when the clamped end of the beam is subjected to harmonic displacements. The theoretical results for the transmissibility are then compared with the measured ones obtained during tests performed on a laboratory in order to assess the validity of the theoretical model proposed.

3. THEORETICAL MODELING

The simplifying hypotheses adopted in the theoretical model proposed here are: (i) the tip mass behaves as a rigid body; (ii) the rotary inertia and shear deformation of the beam may be neglected and (iii) both the beam and tip mass displacements and rotations are small. With the above assumptions, the transverse vibrations of the prototype shown in Fig. 2, in the absence of external forces, are described mathematically by the partial differential Eq. (1) subjected to the boundary conditions described by Eqs. (2), (3) and (4).

$$EI\frac{\partial^4 w(x,t)}{\partial x^4}+\mu\frac{\partial^2 w(x,t)}{\partial t^2}+f_d(t,w,\dot{w})=0 \tag{1}$$

$$w(0,t)=W_0\,\mathrm{e}^{\mathrm{i}\Omega t},\ w'(0,t)=0 \ \text{ at } x=0 \tag{2}$$

$$EI\,w''(L,t)=-\left(J_G+ml^2\right)\ddot{w}'(L,t)-ml\,\ddot{w}(L,t) \ \text{ at } x=L \tag{3}$$

$$EI\,w'''(L,t)=m\,\ddot{w}(L,t)+ml\,\ddot{w}'(L,t) \ \text{ at } x=L. \tag{4}$$

In Eqs. (1)-(4), x denotes the axial coordinate along the beam length; t denotes the time; $w(x,t)$ denotes the transverse displacement field; EI and μ denote, respectively, the bending stiffness and the mass per unit length of the beam; m and J_G denote, respectively, the tip mass and the tip moment of inertia about the gravity center C-G; l denotes the axial distance between the attachment point of the tip mass to the beam and the center of gravity of the tip mass; W_0 and Ω denote, respectively, the amplitude and the circular frequency for the prescribed displacement at the clamped end $x = 0$; and, finally, $f_d(t,w,\dot{w})$ denotes the damping forces. Here and in what follows, the dot and prime symbols over a variable denote, respectively, temporal and spatial derivatives. The bending stiffness of the beam may be computed through the expression:

$$EI=E\frac{\pi\phi_A^4}{64} \tag{5}$$

where ϕ_A denotes the nominal diameter of the beam whereas E is the Young modulus for the steel (E = 209 GPa). Before solving the boundary-value problem given by Eqs. (1)-(4), one must adopt a model for the damping forces. Several models for structural damping are available in the literature; here, as a first investigation, one adopts a quite simple and widely used hysteretic damping model for which one may write

$$f_d(t,w,\dot{w})=\frac{h}{\Omega}\frac{\partial w(x,t)}{\partial t} \tag{6}$$

where the parameter h is commonly referred to as the hysteretic damping parameter. Previous researchers correlate the hysteretic damping parameter with the logarithmic decrement (Wagner *et al.*, 1973), a quantity measured on a laboratory with relatively ease.

With the hysteretic damping model given by Eq. (6), the boundary-value problem defined by Eqs. (1)-(4) becomes linear; hence, one might expect that the steady-state vibrations are also harmonic in time; in other words, the transverse displacement field may be written as

$$w(x,t) = W(x)\,\mathrm{e}^{\mathrm{i}\Omega t}$$

where $W(x)$ denotes the (complex) amplitude of the displacement and i denotes the imaginary unity ($\mathrm{i}^2 = -1$) . Substituting the above expression for $w(x,t)$ into Eqs. (1)-(4) one derives the following boundary-value problem for the complex amplitude $W(x)$:

$$\frac{d^4W(x)}{dx^4} - \left(\frac{\mu\Omega^2 - \mathrm{i}h}{EI}\right) W(x) = 0 \tag{7}$$

$$W(0) = W_0\,,\ W'(0) = 0 \ \text{ at } x = 0 \tag{8}$$

$$EI\,W''(L) = \left(J_G + ml^2\right)\Omega^2\ W'(L) + ml\,\Omega^2\,W(L) \ \text{ at } x = L \tag{9}$$

$$EI\,W'''(L) = -m\,\Omega^2\,W(L) - ml\,\Omega^2 W'(L) \ \text{ at } x = L \tag{10}$$

The analytical solution of the boundary-value problem defined by Eqs. (7)-(10) may be cast in the following form:

$$W(x) = U_1\,\mathrm{e}^{\beta(\Omega)x} + U_2\,\mathrm{e}^{-\beta(\Omega)x} + U_3\,\mathrm{e}^{\mathrm{i}\beta(\Omega)x} + U_4\,\mathrm{e}^{-\mathrm{i}\beta(\Omega)x} \tag{11}$$

where the four components of vector **U** are the solution of a linear system of equations of the kind **KU** = **F**, for which the components of the coefficient matrix **K** and load vector **F** are given by

$$K_{11} = K_{12} = K_{13} = K_{14} = 1\,;\ K_{21} = 1; K_{22} = -1; K_{23} = \mathrm{i}; K_{24} = -\mathrm{i} \tag{12}$$

$$K_{31} = EI\,\beta(\Omega)^2\,\mathrm{e}^{\beta(\Omega)L} - \beta(\Omega)\ \Omega^2\,(J_G + ml^2)\,\mathrm{e}^{\beta(\Omega)L} - ml\,\Omega^2\,\mathrm{e}^{\beta(\Omega)L} \tag{13}$$

$$K_{32} = EI\,\beta(\Omega)^2\,\mathrm{e}^{-\beta(\Omega)L} + \beta(\Omega)\ \Omega^2\,(J_G + ml^2)\,\mathrm{e}^{-\beta(\Omega)L} - ml\,\Omega^2\,\mathrm{e}^{-\beta(\Omega)L} \tag{14}$$

$$K_{33} = -EI\,\beta(\Omega)^2\,\mathrm{e}^{\mathrm{i}\beta(\Omega)L} - \mathrm{i}\beta(\Omega)\ \Omega^2\,(J_G + ml^2)\,\mathrm{e}^{\mathrm{i}\beta(\Omega)L} - ml\,\Omega^2\,\mathrm{e}^{\mathrm{i}\beta(\Omega)L} \tag{15}$$

$$K_{34} = -EI\,\beta(\Omega)^2\,\mathrm{e}^{-\mathrm{i}\beta(\Omega)L} + \mathrm{i}\beta(\Omega)\ \Omega^2\,(J_G + ml^2)\,\mathrm{e}^{-\mathrm{i}\beta(\Omega)L} - ml\,\Omega^2\,\mathrm{e}^{-\mathrm{i}\beta(\Omega)L} \tag{16}$$

$$K_{41} = EI\,\beta(\Omega)^3\,\mathrm{e}^{\beta(\Omega)L} + m\ \Omega^2\,\mathrm{e}^{\beta(\Omega)L} + ml\,\Omega^2\,\beta(\Omega)\,\mathrm{e}^{\beta(\Omega)L} \tag{17}$$

$$K_{42} = -EI\,\beta(\Omega)^3\,\mathrm{e}^{-\beta(\Omega)L} + m\ \Omega^2\,\mathrm{e}^{-\beta(\Omega)L} - ml\,\Omega^2\,\beta(\Omega)\,\mathrm{e}^{-\beta(\Omega)L} \tag{18}$$

$$K_{43} = -\mathrm{i}\,EI\,\beta(\Omega)^3\,\mathrm{e}^{\mathrm{i}\beta(\Omega)L} + m\ \Omega^2\,\mathrm{e}^{\mathrm{i}\beta(\Omega)L} + \mathrm{i}\,ml\,\Omega^2\,\beta(\Omega)\,\mathrm{e}^{\mathrm{i}\beta(\Omega)L} \tag{19}$$

$$K_{44} = \mathrm{i}\,EI\,\beta(\Omega)^3\,\mathrm{e}^{-\mathrm{i}\beta(\Omega)L} + m\ \Omega^2\,\mathrm{e}^{-\mathrm{i}\beta(\Omega)L} - \mathrm{i}\,ml\,\Omega^2\,\beta(\Omega)\,\mathrm{e}^{-\mathrm{i}\beta(\Omega)L} \tag{20}$$

$$F_1 = W_0; F_2 = F_3 = F_4 = 0 \tag{21}$$

and

$$\beta(\Omega) = \sqrt[4]{\frac{\mu\Omega^2 - \mathrm{i}\,h}{EI}}\ . \tag{22}$$

It should be emphasized that when $W_0 = 0$ the boundary-value problem (7)-(10) reduces to a non-self-adjoint eigenvalue problem (Mennicken and Möller, 2003) of the kind **KU** = **0**, for which nontrivial solutions exist if and only if the

determinant of the coefficient matrix **K** is zero. The numerical values of the circular frequency Ω which satisfy the null determinant equation for the coefficient matrix **K** correspond to the natural frequencies of the prototype shown in Fig. 2. Finally, the transmissibility of the prototype, $T(x,\Omega)$, is defined as the ratio between the acceleration at a given location along the beam length and the acceleration imposed at the clamped end $x = 0$; therefore, one may write

$$T(x,\Omega) = \frac{-\Omega^2 W(x)\, e^{i\Omega t}}{-\Omega^2 W_0\, e^{i\Omega t}} = \frac{W(x)}{W_0} = \frac{U_1}{W_0} e^{\beta(\Omega)x} + \frac{U_2}{W_0} e^{-\beta(\Omega)x} + \frac{U_3}{W_0} e^{i\beta(\Omega)x} + \frac{U_4}{W_0} e^{-i\beta(\Omega)x}. \tag{23}$$

A mathematical software was used to compute analytical solutions and Figures (3) and (4) show the transmissibility results derived from Eq. (23) at the two measurement points selected during the experimental tests with the prototype, namely, point 1 at $x = L + C/2$ and point 2 at $x = L/2$ (details about the experimental tests will be described in section 4). The transmissibility results shown in Figs. (3) and (4) are computed for excitation frequencies ranging from 5 Hz to 5.605 kHz with a frequency resolution of 6.25 Hz, which is the frequency resolution adopted in the experimental tests. Moreover, in the computations performed with Eq. (23), the hysteretic damping coefficient is set equal to zero. The first, second, third and fourth natural frequencies calculated analytically are, respectively, 61 Hz, 741 Hz, 2.35 kHz and 5.51 kHz and correspond to the frequencies associated with the four peaks shown in Figs. (3) and (4).

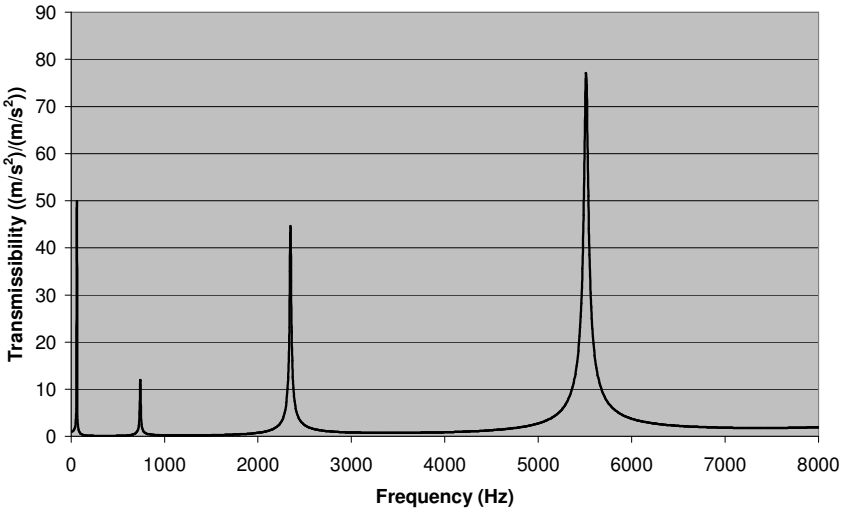

Figure 3. Transmissibility at the mass position (position 1, $x = L+C/2$) obtained with the theoretical model.

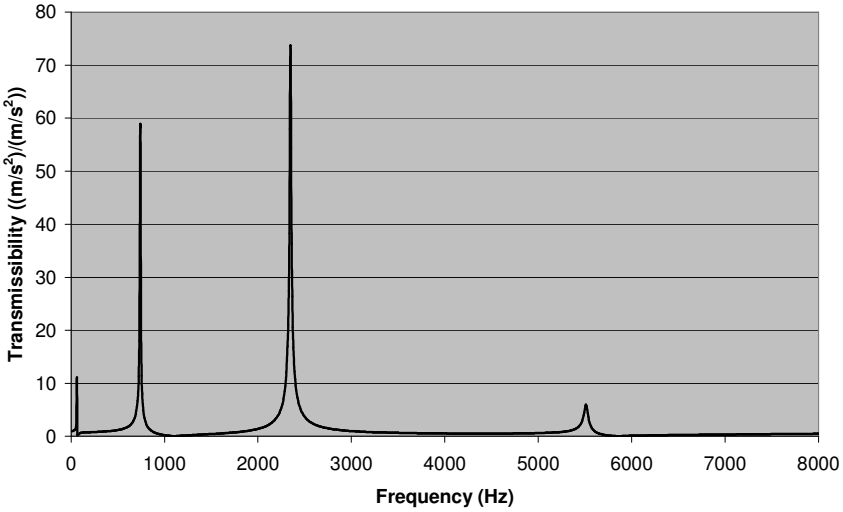

Figure 4. Transmissibility at the beam midpoint (position 2, $x = L/2$) obtained with the theoretical model.

4. NUMERICAL SIMULATION

The prototype was modeled and simulated to understand its behavior when exposed to harmonic functions. The finite element software ANSYS was used with this purpose as it is commercially sated to find mechanical vibrations, frequency response function and frequency modes.

The dimensions shown on table 1 were used to manufacture the prototype and also as input for the tridimensional numerical simulation.

The material for the prototype was assumed as an elastic isotropic material with elastic module E= 209GPa and specific weight ρ= 7860kg/m³. *Solid Brick 8 node 45* was used for the 3-D mesh modeling. This element type is defined by eight nodes and three degrees of freedom for each node. The element has plasticity, creep, swelling, stress stiffening, large deflection, and large strain capabilities.

The mathematic method used by the software on this simulation was the *Full method* due to its simplicity and its completeness compared to the other two methods available on ANSYS (reduced method and modal superposition method). This method makes use of the full stiffness and mass matrices and thus is the slower and costlier option. The tetragonal mesh was used.

The boundary restrain conditions used to the simulation had the objective to approximate to the experimental situation. The beam was fixed by the smaller diameter and this basis had a prescribed harmonic displacement. Several different forced frequencies were used between the range of frequency from 5 to 6000Hz with a frequency resolution (sub-step) of 22 Hz. For each frequency the simulation was performed and the transmissibity for the range was analyzed.

On Figure 5 can be seen the forth first modes. The first and second models dissipate bending energy. The third mode compress the beam and the forth mode dissipates a torsion elastic energy.

On Figures 6 and 7 the relative displacement of two points located on the beam in respect to the prescribed displacement boundary. Analyzing those Figures, it can be considered that 60, 750, 2300 and 5300 Hz were taken as natural frequencies related to the four modes.

On Figure 6, the transmissibity taken on the mass (x=L+C/2) is presented and it can be noted that the higher amplitude was on the forth natural frequency. On Figure 7, the transmissibility related to a point located on the middle of the messenger cable and it can be noted that only two frequencies had a higher response.

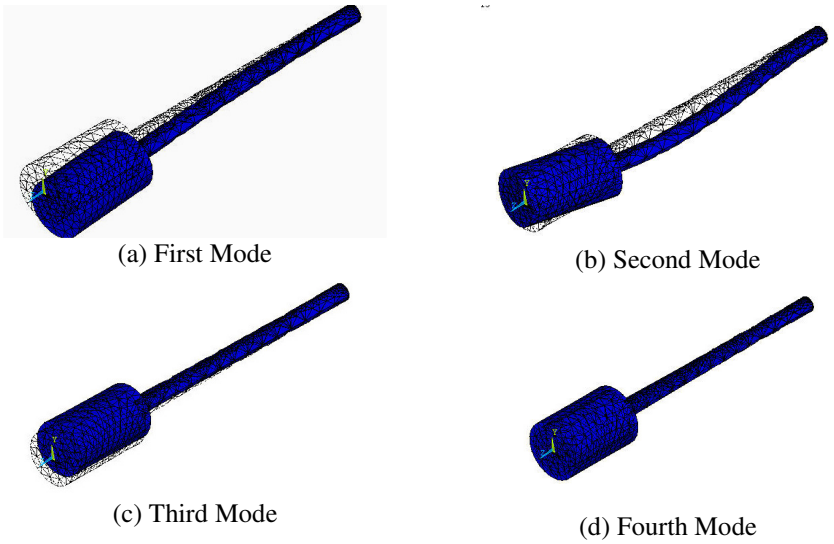

(a) First Mode (b) Second Mode

(c) Third Mode (d) Fourth Mode

Figure 5. The first four natural modes of vibration for the prototype investigated.

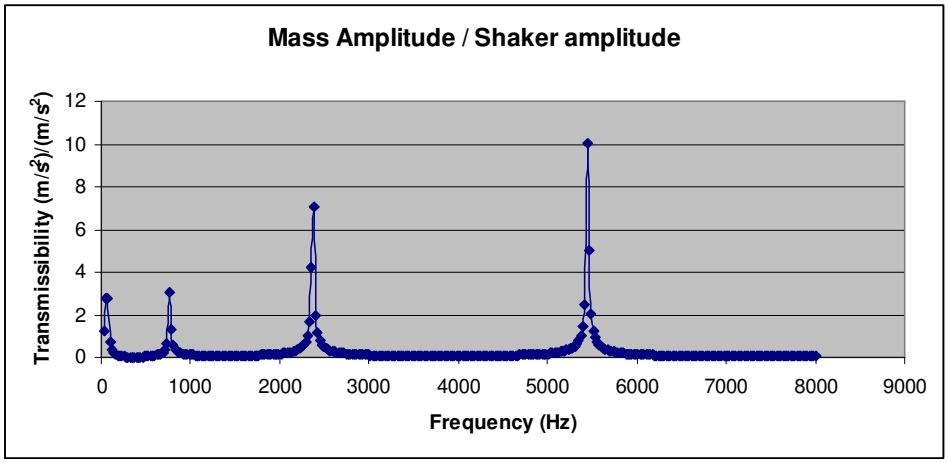

Figure 6 - Transmissibility at the mass midpoint (position 1, $x = L + C/2$) obtained with the numerical model.

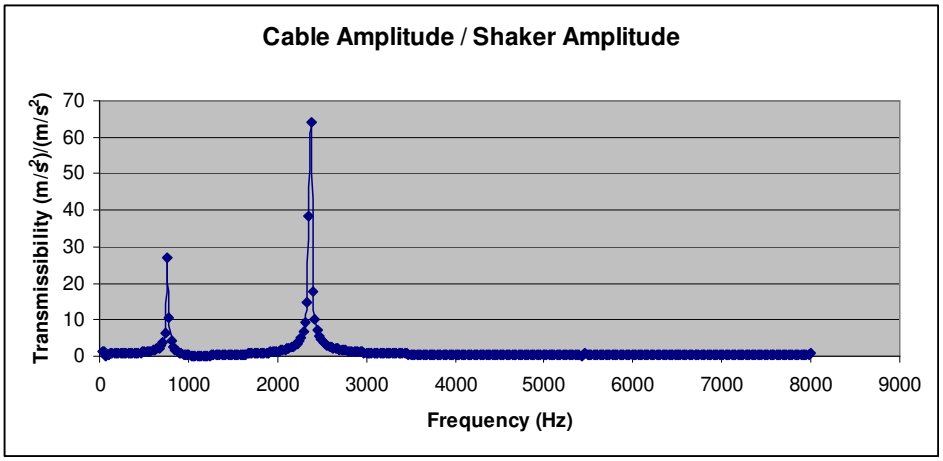

Figure 7. Transmissibility at the beam midpoint (position 2, $x = L/2$) obtained with the numerical model.

5. EXPERIMENTAL TESTS

Experimental tests were performed with the prototype on a laboratory in order to compare the analytical and numerical results obtained for its transmissibility with the corresponding measured ones. The prototype was mounted on an electrodynamics shaker and three piezoelectric accelerometers were fixed on different positions for measurements of the excitation acceleration and response accelerations. Figure 8 illustrates a schematic view of the experimental apparatus for the laboratory tests performed.

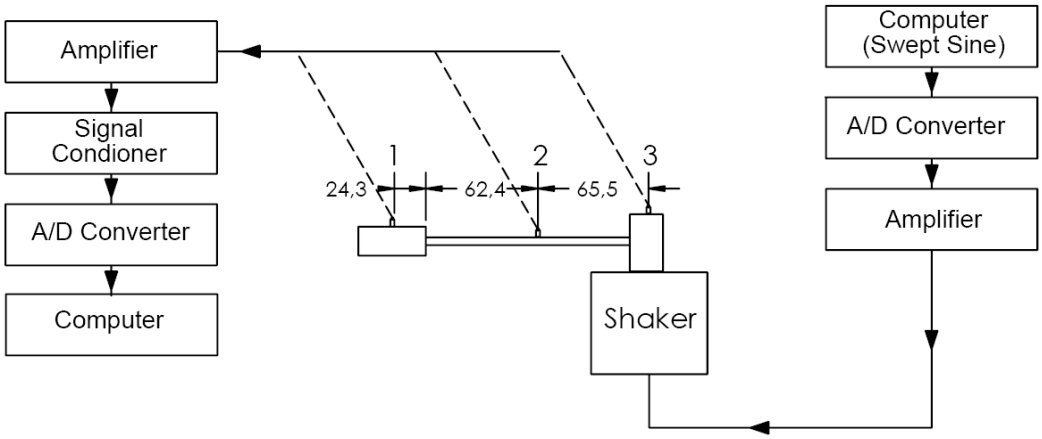

Figure 8 - Experimental set-up.

As indicated on Fig. 8, the accelerometers labeled as 1, 2 and 3 and attached to the prototype were electrically connected to an amplifier, a signal conditioner, an analogical-digital converter. The digital signals measured by the accelerometers were collected by the computer. The prototype was fixed at the shaker which transformed the amplified signal from the computer and a Digital-analogical converter to mechanical oscillations.

The selected excitation signal generated by the computer was a swept sine, that is, a harmonic waveform with variable frequency. The swept sine had 200mV RMS amplitude and its frequency changes from 5 Hz to 8 kHz with a linear sweep rate equal to XX Hz/s. The measured transmissibility at a given position was computed from the cross-correlation function between the acceleration imposed at the clamped end and the acceleration measured at that position. Thirty independent samples of the acceleration signals in the time domain were used to compute the average cross-correlation function.

In Figs. 9 and 10, one illustrates graphically the ratio between the acceleration amplitudes at the measurement points 1 and 2 and the acceleration amplitude at the clamped end (point 3) as a function of the excitation frequency. Three natural frequencies noted on experimental results were 62,5, 75* Hz, 675* Hz, 900Hz, 2800 Hz and 3370 Hz. (* only in Figure 9)

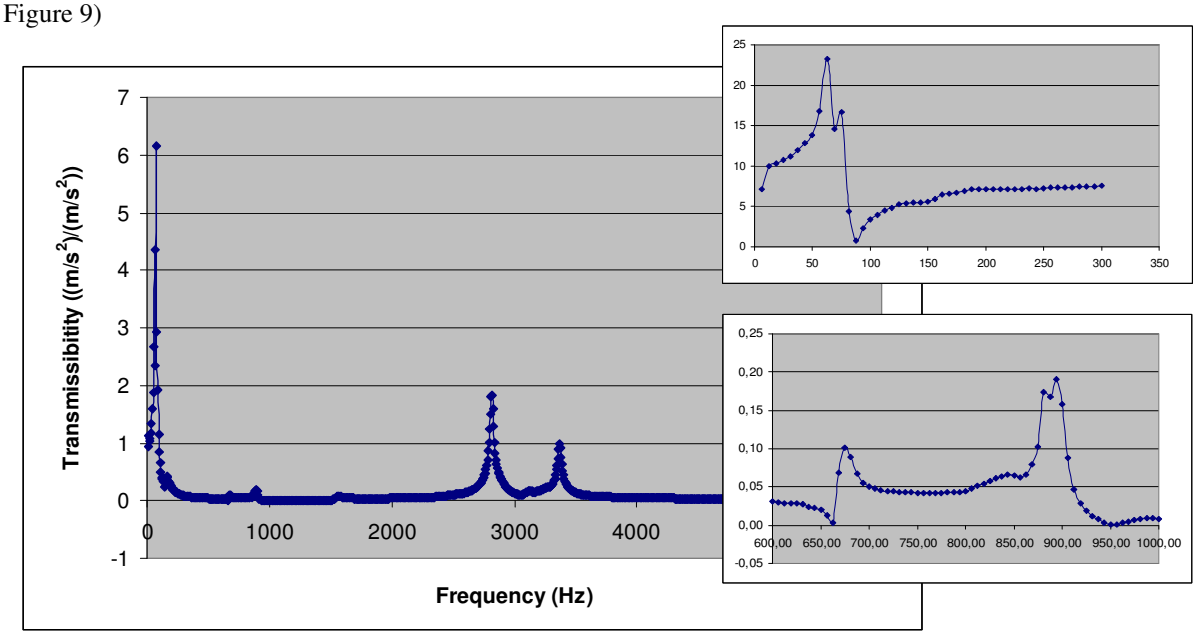

Figure 9 –Transmissibility at point 1 obtained experimentally.

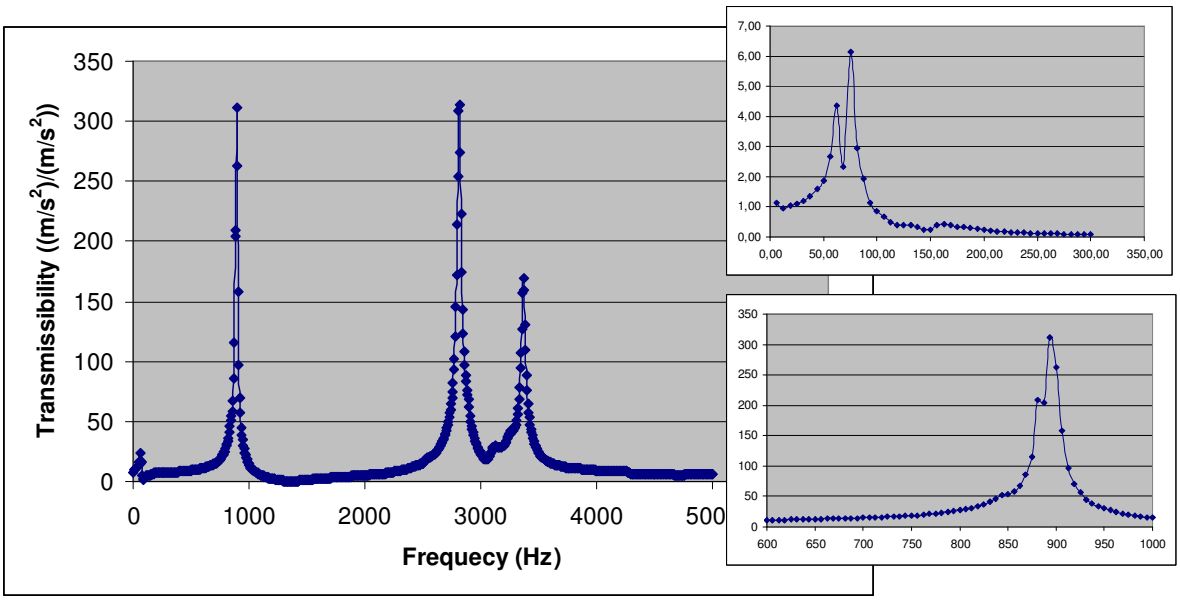

Figure 10 – Transmissibility at point 2 obtained experimentally.

6. CONCLUSIONS

In this work a prototype comprising a cantilever beam carrying a tip mass at the free end and resembling a typical Stockbridge damper was manufactured and tested on a laboratory. The prototype tested had not the exact geometrical shape of a typical Stockbridge damper and the uniform cantilever beam had geometric, stiffness and damping properties different from the corresponding ones of a typical messenger cable. The experimental tests were designed in order to identify the natural frequencies of the prototype and to measure its transmissibility when the clamped end of the cantilever beam was subjected to forced harmonic displacements in a wide frequency range. With an analytical one-dimensional continuous Euler-Bernoulli beam model and a full three-dimensional numerical model one computed the natural frequencies and the transmissibility for further comparison with the corresponding measured data. The analytical and numerical results obtained for the natural frequencies and transmissibility did not take into account the damping effects in the prototype. Table 2 presents the measured, analytical and numerical results for the first four natural frequencies of the prototype.

Table 2. Measured, analytical and numerical results for the first four natural frequencies of the prototype.

Natural Frequencies	Analytical Results	Numerical Results	Experimental Results
1	61 Hz	60 Hz	62.5 Hz / 75* Hz
2	741 Hz	750 Hz	675* Hz / 900 Hz
3	2.35 kHz	2.3 kHz	2.75 kHz
4	5.51 kHz	5.30 kHz	3.30 kHz

From the analysis of Tab. 2 one may draw the following conclusions. First, the analytical and numerical results for the first four natural frequencies of the prototype are in very good agreement; the maximum relative error between them is less than 4%. For the first natural frequency the three models were almost coincident. However, large discrepancies are verified when both the analytical and numerical results for the second, third and fourth natural frequencies when compared with the corresponding measured ones. The second, the third and the fourth natural frequencies of the prototype by, respectively, at least 20%, 17% and 61% were both the analytical and numerical models underestimate.

The first mode is the one that the accelerometer was positioned to measure, as it can be seen on Figure 5(a) and 8. It should be investigate the possibility of taking more data with other sensors and analyze the complexity of all the modes and displacements.

Concerning the transmissibility results, from the analysis of Figs. 3, 4, 6, 7, 9 and 10, one may conclude that both the analytical and numerical results reproduce qualitatively the dynamic behavior of the prototype verified experimentally on a laboratory (one may note the remarkable agreement between the plots shown in Figs. 4 and 10 in the frequency range from 0 to 1 kHz); nevertheless, quantitatively, both the analytical and numerical models are unable to reproduce the magnitudes of the transmissibility measured at the positions 1 and 2. The reasons for the large discrepancies might be attributed to the neglect of damping effects in the preliminary theoretical investigations performed in the current work. Because both the analytical and numerical transmissibility are computed for no damping, their magnitudes change appreciably depending on the frequency resolution. The authors recognize that much more research efforts must be done both theoretically and experimentally for more conclusive remarks about the validity of the theoretical models proposed and will be the subject of future investigations.

AKNOWLEDGEMENTS

The authors acknowledge the support of CEFET/RJ, CEPEL, Brazilian Research Councils CNPq and FAPERJ.

REFERENCES

Bhat, B.R. and Wagner, H., 1975, “Natural Frequencies of a Cantilever with a Tip Mass Slender in Axial Direction”, Department of Mechanical Engineering, University of Dar-Es-Salaam, Vikram Sarabhai Space Center.

Durvasula, S., 1965, “Vibrations of a Uniform Cantilever Beam Carrying a Concentrated Mass and Moment of Inertia and a the Tip”, Report AE 1338, Department of Aeronautical Engineering, Indian Institute of Science, Bangalore.

Hagedorn, P., “On the computation of damped wind-excited vibrations of overhead transmission lines”, Journal of Sound and Vibration, Vol. 83, No. 2, pp. 253-271, 1982.

International Standard, 1997, “Overhead Lines- Requirements and Test for Fittings”,2ºEd. CEI, IEC61284.

Karnopp, B., 2000, ”Dynamics and Vibratins”, Ed.Richard C. Dorf Boca Raton: CRC Press LLC,

Mennicken, R. and Möller, M., “Non-self-adjoint boundary eigenvalue problems”, North-Holland Mathematics Studies 192, 2003, 500p.

Parnell, L.A. and Cobble, M.H., 1975, "Lateral Displacement of a Vibrating Cantilever Beam with a Concentrated Mass", Jornal of Sound and Vibration, Department of Mechanical Engineering, New Mexico88003,U.S.A. 44(4), pp.499-551,

Pipes, L.A., 1985, "Applied Mathematics for Engineers and physicists", Ed. McGraw-Hill Book Company,Inc, New York.

Prescott, J., 1946, "Applied Elasticity", Dover Publications, New York.

Prodonoff, V.,1990, "Mechanical Vibration: Simulation and Analyze", Ed. Maity Comunicação, Rio de Janeiro, Brazil,

Rama Bhat, B. and H. Wagner 1975 Department of Mechanical Engineering, University of Dar-Es-Salaam, Vikram Sarabhai Space Center. Natural frequencies of a cantilever with a tip mass slender in axial direction.

Silva, V.P., 2006, "Numerical and Experimental Investigation of Stockbridge Damper at Overhead Line", Curitiba, Brazil

Temple, G. and Bickley, W.G., 1956, "Rayleigh's Principle", Dover Publications, New York.

Varella, A. V., Matt, C. F. and Cavalcanti, E. S. C., Experimental investigation of the dynamic behavior of Stockbridge dampers, Proceedings of the 18th International Congress of Mechanical Engineering (COBEM), November 6-11, 2005, Ouro Preto, MG, Paper 1991.

Wagner H., Ramamurti, V., Sastry, R.V.R. and Hartmann, K., 1973, "Dynamics of Stockbridge Damper", Jornal of Sound and Vibration, Departament of Applied Mechanics, Indian Instituite of technology, 30(2), pp. 207-220.

RESPONSIBILITY NOTICE

The authors are the only responsible for the printed material included in this paper.